http://dx.doi.org/10.5516/NET.06.2013.082

SEPARATION OF CsCl FROM LiCl-CsCl MOLTEN SALT BY COLD FINGER MELT CRYSTALLIZATION

JOSHUA R. VERSEY[1], SUPATHORN PHONGIKAROON[2*], and MICHAEL F. SIMPSON[3]
[1]Department of Chemical and Materials Engineering and Nuclear Engineering Program University of Idaho
Center for Advanced Energy Studies, 995 University Blvd, Idaho Falls, ID 83401 USA
[2]Department of Mechanical and Nuclear Engineering Virginia Commonwealth University
401 West Main Street, Room E3253 P.O.Box 843015 Richmond, VA 23284-3015
[3]Department of Metallurgical Engineering University of Utah
135 South 1460 East, Salt Lake City, Utah 84112 USA
[*]Corresponding author. E-mail : sphongikaroon@vcu.edu

Received September 24, 2013
Accepted for Publication February 12, 2014

This study provides a fundamental understanding of a cold finger melt crystallization technique by exploring the heat and mass transfer processes of cold finger separation. A series of experiments were performed using a simplified LiCl-CsCl system by varying initial CsCl concentrations (1, 3, 5, and 7.5 wt%), cold finger cooling rates (7.4, 9.8, 12.3, and 14.9 L/min), and separation times (5, 10, 15, and 30 min). Results showed a potential recycling rate of 0.36 g/min with a purity of 0.33 wt% CsCl in LiCl. A CsCl concentrated drip formation was found to decrease crystal purity especially for smaller crystal formations. Dimensionless heat and mass transfer correlations showed that separation production is primarily influenced by convective transfer controlled by cooling gas flow rate, where correlations are more accurate for slower cooling gas flow rates.

KEYWORDS : Pyroprocessing, Cold Finger, Crystallization, Fission Product, Separation

1. INTRODUCTION

Electrolytic oxide reduction is the head end process of pyroprocessing technology that enables the process to accommodate reprocessing of any oxide fuels (e.g. UO_2) (see Fig. 1). This process involves the use of a cathode, anode, and electrolyte to reduce oxide fuel to metallic form. The electrolyte is a lithium chloride - lithium oxide ($LiCl-Li_2O$) salt which becomes contaminated over time with fission products that diffuse from the used nuclear fuel into the electrolyte during operation (see Fig. 2) [1].

Here, a cold finger crystal growth separation is proposed as a method for removing fission products from oxide reduction electrolyte in an effort to reduce nuclear waste volume. This method is similar to a melt crystallization process called layer crystallization that results in solidification and removal of purified electrolyte on a cooled wall. Layer crystallization was proposed and explored by the Korea Atomic Energy Research Institute (KAERI) and was experimentally proven to minimize the amount of lithium chloride (LiCl) salt waste [2]. Melt crystallization techniques are based on principles of thermodynamic phase change and phase equilibrium. Here, the cold finger is cooled to the melting temperature of LiCl (605˚C) to selectively freeze LiCl to the cold finger so it can be removed as purified

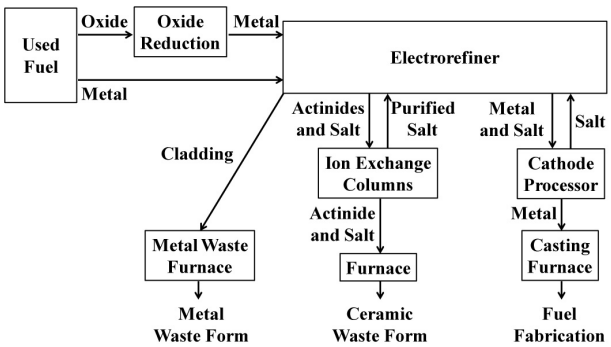

Fig. 1. Conceptual Diagram of Proposed Advanced Pyroprocessing Technology with Oxide Reduction.

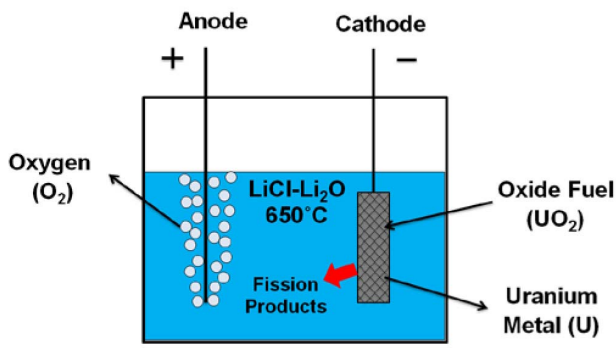

Fig. 2. Diagram of the Oxide Reduction Process of Reducing Oxide Fuel to Metal form.

electrolyte [3]. From that information, the separation theory is best described with the use of a binary phase diagram of lithium chloride - cesium chloride (LiCl-CsCl) provided by Fact-Sage [4] (see Fig. 3). The binary phase diagram includes additional figures that show how molten salt electrolyte is concentrated with cesium chloride (CsCl) as LiCl is selectively removed, via the cold finger, over time. An initial time and concentration of CsCl is depicted as stage one. Stage two represents an intermediate time where the molten salt is more concentrated having a lower liquidus temperature. Stage three would be the final time where a relatively pure LiCl crystal is removed from the CsCl concentrated melt for reuse. The cold finger was designed to have a controlled surface temperature that targets the liquidus melting temperature of a given molten salt composition in order to selectively freeze out LiCl from contaminated oxide reduction electrolyte. KAERI has shown for their similar process of layer crystallization that 90% of processed electrolyte can be recycled back to the electrolytic oxide reduction process at crystal growth rates less than 5 g/min with at least 90% LiCl electrolyte purity [2].

Despite a successful demonstration of this technique by KAERI, there are still missing fundamental aspects to be explored such as heat and mass transfer, providing the motivation to study this method in order to optimize the process and safely reduce oxide reduction electrolyte waste. The main goal is to develop a fundamental understanding of the processes involved with the cold finger method in order to optimize the separation of CsCl from a LiCl electrolyte. To achieve this goal, experiments have been performed with various combinations of varying initial CsCl concentrations, cold finger coolant flow rates, and separation times. In addition, dimensionless correlations that take the form of a conventional Nusselt or Sherwood correlation for a natural convective system have been proposed and fitted to the experimental data to better understand crystal growth rate behavior and determine the rate controlling

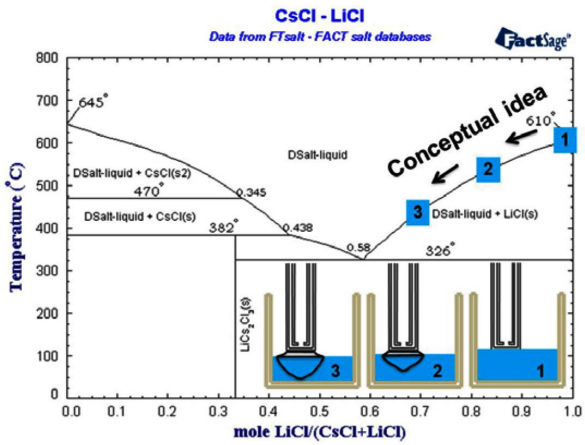

Fig. 3. Fact-Sage LiCl-CsCl Binary Phase Diagram [4] with Conceptual Idea of the Cold Finger Crystal Growth Process.

physics of the cold finger process. It is anticipated that this study will contribute to waste volume minimization of pyroprocessing technology by recycling purified electrolyte which also reduces the cost for reprocessing used nuclear fuel.

2. EXPERIMENTAL PROGRAM

While in the oxide reduction process, a LiCl-Li_2O electrolyte is used, the Li_2O was left out of this study because of its low concentration (1-3 wt%) and to simplify the experiments [1, 5]. To further simplify the system, non-radioactive CsCl was selected to represent all Group I/II fission products because of its abundant accumulation in the oxide reduction electrolyte [1]. The other fission product present in the LiCl electrolyte in high concentrations is strontium (Sr). Future work in this area would logically include the study of salts containing both CsCl and strontium chloride ($SrCl_2$). The experimental equipment was set up in an MBraun glovebox providing an inert argon gas atmosphere (O_2 and moisture levels below 5 ppm). The experimental set up consists of an Air Gas flow meter, custom cold finger, Idaho Laboratory type-K thermocouples, Ozark Technical Ceramics magnesium oxide (MgO) crucible, Kerr Electro-Melt furnace, and type-K Omega thermometers. The chemicals used were Alfa Aesar 99.9% lithium chloride salt (LiCl CAS#: 7447-41-8) and Aldrich Chemistry high-purity cesium chloride salt (CsCl CAS#: 7647-17-8). The tip of the cold finger is cooled to the freezing temperature of LiCl via flow through of argon gas that is regulated by the flow meter. The cold finger is placed in the crucible containing 30 g of molten salt so its tip is flush with the molten salt contained by the crucible measuring 5.1 cm in diameter and 5.1 cm in height (see Fig. 4). The molten salt in the crucible measured approximately 12 mm in depth. The experiments were operated and controlled at 650˚C, which is the same operating temperature for the oxide reduction process.

Table 1 provides the summary of all experimental runs. Five initial salt compositions of CsCl (0, 1, 3, 5, and 7.5 wt%) were explored under different conditions. Exp. No. 1a was done by varying crystal growth separation time (1, 2, 3, 4, 5, 10, 15, 30, and 60 min) at a constant cooling gas flow rate of 11.0 L/min. Exp. No. 1b was performed by fixing the crystal growth time at 30 min and varying the cooling gas flow rate (5.1, 6.2, 6.8, 7.4, 8.5, 9.8, and 11.0 L/min). These two experiments provided an experimental base line and operational limitations. Exp. No. 4 was with an initial 5 wt% CsCl in LiCl for various separation times (5, 10, 15, and 30 min) and cooling rates (7.4, 9.8, 12.3, and 14.9 L/min) exploring optimum cold finger separation operating variables. The other series of experiments varied cooling rate (7.4, 9.8, 12.3, and 14.9 L/min) at a constant crystal growth time of 15 minutes (Exp. Nos. 2, 3, and 5).

Methods for nondestructive and destructive mass and dimension measurements were developed. The masses of both the cold finger with crystal and the crucible with bulk salt were measured to determine the crystal mass growth rate and the remaining concentrated bulk salt mass. Dimensions a, b, d, and e, as indicated in Fig. 5, were measured to locate the solid/liquid surface area interface throughout the crystal growth process. Dimension "c" was measured later once a portion of the crystal's edge was chipped away from the cold finger. The white portion of the crystal drip was removed by a machining file (see Fig. 5). The cold finger and crystal mass was measured again without this portion of the drip. The double hatch mark portion was assumed to be only the drip whereas the single hatch mark section represents a drip affected region of the purified crystal. The region with no hatch mark is considered to be purified LiCl crystal. A portion of the crystal's edge was now chipped away and dimension "c" could then be measured. The rest of the crystal was chipped away from the cold finger and crushed in a mortar and pestle to small granules. All collected samples of all sections were analyzed by Inductively Coupled Plasma Mass Spectrometry (ICP-MS). The post processing of purified crystals required 3 to 4 hours.

The sample preparation for an ICP-MS elemental analysis involved three basic analytical routines for (1) the bulk sample from the CsCl concentrated bulk salt at the end of experiments, (2) the drip on the crystal being removed from the crystals, and (3) the crystal without the drip. Exception was made for experiments with initial concentration of 5 wt% CsCl where the sample came from the entire crystal including the drip. The samples were digested in 3 mL of nitric acid (HNO_3). After that, 10 mL of 18 mΩ nanopure water was added to the digested samples, which were then agitated to ensure a homogenous mixture. Then 50 μL of the solution was diluted 241 times by adding 12 mL of 18 mΩ nanopure water. After that, 1 mL of this solution was diluted 10 more times by adding 9 mL of 5% HNO_3. This final diluted sample was then analyzed for elemental composition of lithium (Li) and cesium (Cs). Uncertainty associated with the ICP-MS measured value is in the range of 10%.

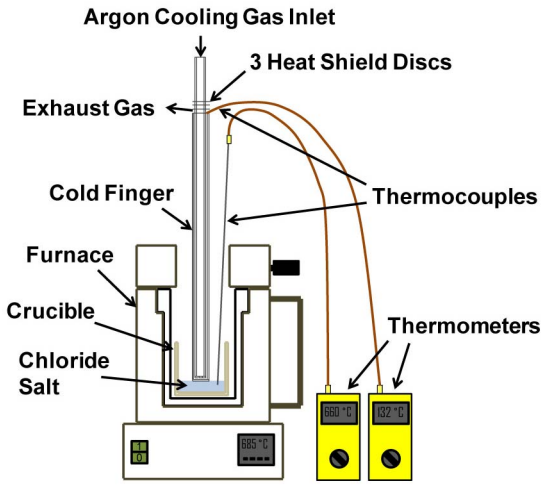

Fig. 4. Cutaway Diagram of Experimental Setup.

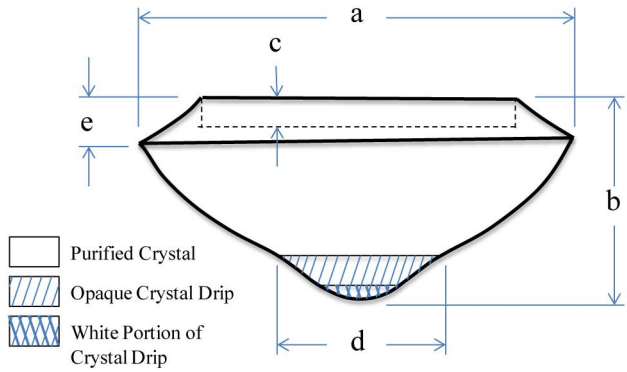

Fig. 5. Experimental Crystal Representation showing Color Regions and Dimensions that were Measured. "a" is the Crystal's Overall Diameter, "b" is the Crystal's Overall Height, "c" is the Height the Crystal Grow Up the Side of the Cold Finger, "d" is the Opaque Film Diameter of Concentrated Bulk Salt that Freezes at the Bottom of the Crystal in the form of a Drip, and "e" is the Distance between the Crystals Highest Point Up the Side of the Cold Finger and its Point of Largest Diameter.

Table 1. Outline of Experiments Performed for this Work

Exp. No.	Initial LiCl-CsCl Concentration (wt% CsCl)	Crystal Growth Time (min)	Cooling Gas Flow Rate (L/min)
1a	0	1 – 60	11.0
1b	0	30	5.1 – 11.0
2	1	15	7.4 – 14.9
3	3	15	7.4 – 14.9
4	5	5 – 30	7.4 – 14.9
5	7.5	15	7.4 – 14.9

3. RESULTS AND DISCUSSION

3.1 Crystal Growth Data Sets

The initial 5 wt% CsCl concentration in LiCl was selected as a representative concentration that would be found in electrolytic oxide reduction electrolyte that is due for replacement or purification [1]. Fig. 6 shows the effects of crystal growth time and cooling gas flow rate on crystal growth and purity of Exp. No. 4.

Fig. 6 shows both *assumed and experimental* highest and lowest concentrations with white arrows and underlined data, respectively. Here, *assumed* concentrations were based on ideal assumptions for thermodynamic equilibrium before experiments were performed and compared with actual results of experiments. The grown crystal mass was assumed to increase as both crystal growth time and cooling gas flow rate increase. The highest CsCl concentration for purified crystals was assumed to be the experimental crystal with the shortest growth time and largest cooling gas flow rate (see white arrow pointing upward in Fig. 6). The lowest CsCl concentration for purified crystals was assumed to be the experimental crystal with the longest crystal growth time and smallest cooling gas flow rate (see white arrow pointing downward in Fig. 6). The experimental crystal growth rate matched assumed results, but the experimental purified crystal concentration did not match assumed results. The theory of phase equilibrium as it relates to crystal purity guided the intuition of crystal concentrations. The theory states that (1) if a salt system is at equilibrium throughout an entire experiment the crystal would be 100% pure and (2) if forced from equilibrium by heat removal the salt system impurities would freeze with pure species before the system could return to an equilibrium state [6]. The impure and pure species freeze together because the heat removal occurs faster than the diffusion of impure species away from pure species, so higher cooling rates would result in higher impurity concentrations. Contrary to the assumed crystal concentrations, the highest CsCl concentration was for the experimental crystal (Exp. No. 4) with the shortest growth time (5 min) and smallest cooling gas flow rate (7.4 L/min) and the lowest CsCl concentration was for Exp. No. 4 with 15 min growth time and 9.8 L/min cooling gas flow rate shown as underlined data in Fig. 6.

Detailed observation of the crystal formations reveals a potential explanation for why the *experimental* crystal concentration results are different from the expected results. The assumption with the expected guess was based on the following two reasons: (1) the crystal was formed only while submerged in the molten salt during cold finger operation and (2) there was no bulk salt residue on the crystal when removed from the molten salt. It was discovered that crystal mass formed during cold finger operation was transparent and crystal formed during a more rapid cool down was opaque. An examination of each crystal showed that a portion of the crystal, shaped in the form of a drip, was opaque indicating that bulk salt residue was removed with crystals (see Fig. 7). Fig. 7 shows a side and bottom view of a pure LiCl and LiCl-CsCl experiment at a common growth time of 30 min and a cooling gas flow rate of 11.0 L/min. The most likely cause for the opaque coloring of the drip is that it freezes faster than the rest of the crystal formed during normal cold finger operation, creating more grain boundaries in its formation.

A potential explanation for the unexpected concentrations is that the drip was formed with CsCl concentrated bulk salt that froze to the crystal as the cold finger and crystal were removed from the concentrated molten salt. This explains why the smaller crystals have higher CsCl concentrations; because the mass fractions of the CsCl concentrated drip is large for smaller crystals and smaller for larger crystals. This change in mass is due to the diffusive and convective effects of heat and mass transfers. The heat transfer between the pure LiCl and LiCl-CsCl experiments would be similar,

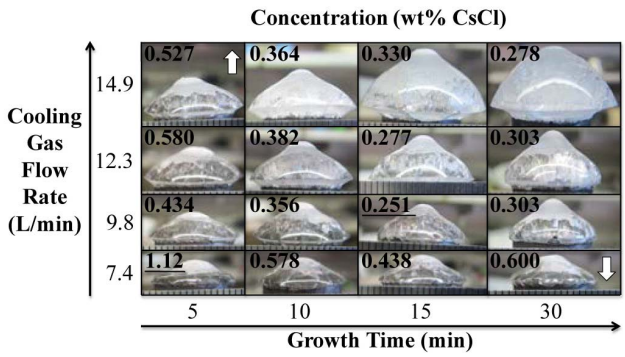

Fig. 6. Crystal Concentration Results for Experiments Performed at an Initial Bulk Concentration of 5 wt% CsCl in LiCl. CsCl Concentrations Reported as wt% CsCl are Located on the Upper Left Hand Corner of Each Image and were Calculated with Mole Balances using Raw ICP-MS Data for Li and Cs.

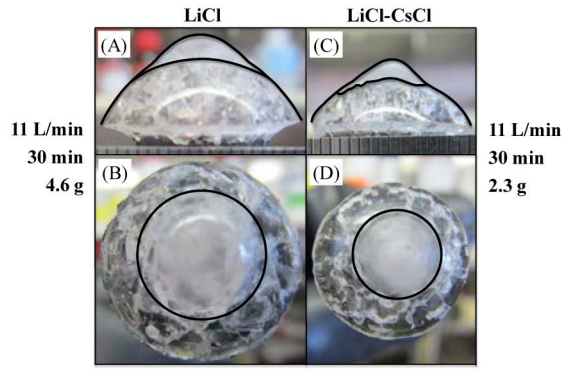

Fig. 7. Crystal mass Comparison for Pure LiCl (A and B) and LiCl with an Initial 5 wt% CsCl (C and D) at the Same Cold Finger Operating Conditions and Parameters with Lines Highlighting an Opaque Residue Drip Formation (Black Lines). The Crystal Mass for LiCl-CsCl Decreases by One Half the Crystal Mass for Pure LiCl at the Same Cold Finger Operating Conditions and Parameters.

suggesting that the primary reason for the decrease in crystal mass for the LiCl-CsCl experiment is a lower melting point at the crystal surface affected by mass transfer as CsCl moves into the bulk via convection and diffusion.

Next, the crystal and drip mass data for pure LiCl and LiCl-CsCl with 5 wt% CsCl experiments were plotted versus growth time to show the effect of both cooling rate and initial CsCl concentration (see Fig. 8). As expected the mass versus time plot shows an increase in crystal mass as crystal growth time increases. Each of the mass profiles follows uniform and predictable exponential trends that increase linearly in magnitude with increasing cooling gas flow rate. The mass profiles for 5 wt% CsCl experiments at 7.4, 9.8, and 12.3 L/min cooling gas flow rates all appear to reach a steady state crystal and drip mass within 30 min of crystal growth time. The crystal and drip data series for pure LiCl includes masses for crystal growth times ranging from 1 to 60 min, which gives an idea of projected mass versus time profiles for experiments with 5 wt% CsCl in LiCl.

The concentration data for initial 5 wt% CsCl in LiCl experiments were analyzed to discover optimum cold finger crystal growth operating parameters. This is the time at the lowest CsCl concentration. Fig. 9 shows a representative plot of crystal and drip concentration versus crystal growth time that shows a CsCl concentration minimum at a growth time of 15 min for three of the four cooling gas flow rate data series. The other data series had a minimum CsCl concentration at a 30 min growth time. However, it is possible within uncertainty to have a minimum at a 15 min growth time for this data series. So within uncertainty, ranging from ±0.039 to ±0.074 wt% CsCl, the optimum growth time is 15 min for the cooling rate data sets. This information was used to determine an optimum cooling gas flow rate.

Here, both crystal purity and production rate must be considered to make a well rounded economical selection. Fig. 10 shows the effect of these parameters and two possible potential optimum values for cooling gas flow rate. If separation purity is more important, the optimum cooling gas flow rate would be the data point with the lowest CsCl concentration (Exp. No. 4 with 15 min growth time and 9.8 L/min cooling gas flow rate) producing 0.12 g/min at 0.25 wt% CsCl. If separation production rate is more important, the optimum cooling gas flow rate would be the data point with the highest crystal growth rate (Exp. No. 4 with 15 min growth time and 14.9 L/min cooling gas flow rate) producing 0.36 g/min at 0.33 wt% CsCl. Assuming separation production rate is more important than separation purity due to the relatively low CsCl concentrations of data at optimum crystal growth time of 15 min, the optimum cooling gas flow rate was selected to be 14.9 L/min.

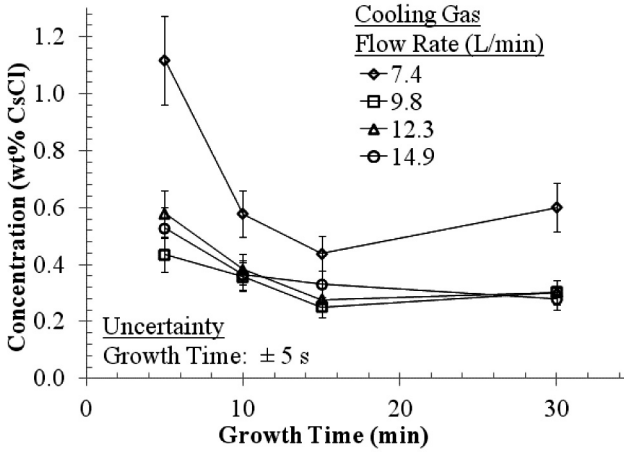

Fig. 9. Purified Crystal and Drip Concentration vs. Crystal Growth Time for Initial 5 wt% CsCl in LiCl for Varying Cooling Gas Flow Rates.

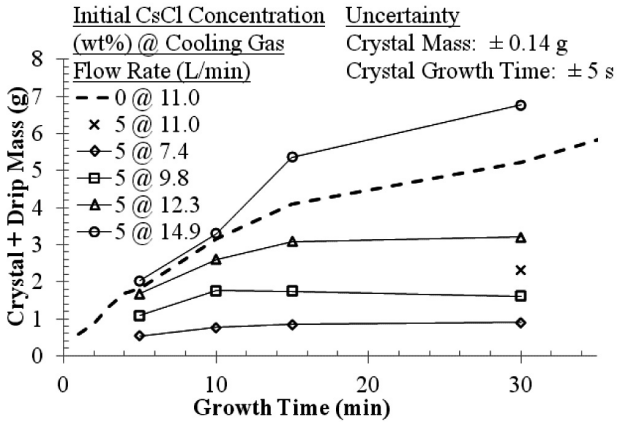

Fig. 8. Mass vs. Time for Purified Crystal and Drip with an Initial 5 wt% CsCl in LiCl for Varying Cooling Gas Flow Rates Compared to Pure LiCl Experiments at a Cooling Gas Flow Rate of 11.0 L/min.

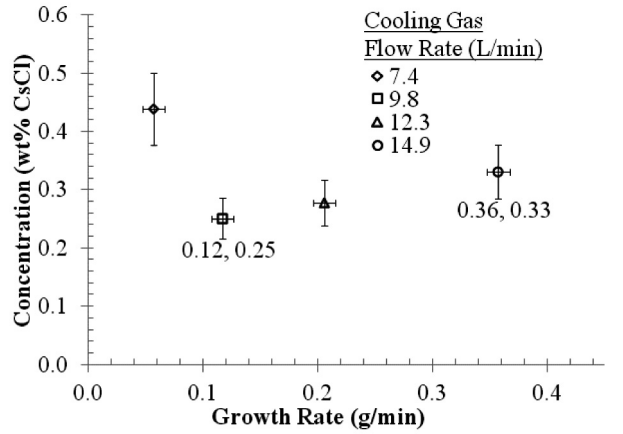

Fig. 10. Purified Crystal and Drip Concentration vs. Crystal Growth Rate for Initial 5 wt% CsCl in LiCl and 15 min Crystal Growth Times for Varying Cooling Gas Flow Rates.

Effects of CsCl concentrated crystal drip formation on purified crystal concentration and effects of initial CsCl concentration on crystal growth rate and purity were both investigated. The concentrated crystal drip formation was assumed to be approximately the same concentration as the concentrated bulk and a plot of crystal drip versus concentrated bulk supports this assumption (see Fig. 11). Moreover, the plot shows that some crystal drip concentrations are higher and some lower than the concentrated bulk concentration. The diagonal line in the plot represents equality between drip and bulk concentrations; that is, the data set that lies above the line indicates that the drip has a higher CsCl concentration than the bulk and vice versa. A potential explanation for data set that lies below the line is in the procedure for removing the crystal drip, while data that lies above the line is due to a diffusion boundary layer at the solid liquid interface of the crystal during cold finger operation. When the purified crystal is removed from the concentrated bulk, the diffusion boundary layer contained in a thin film is removed with the crystal; thus, it freezes to the purified crystal surface before it can drip away from the cooling crystal. Within the diffusion boundary layer, there must be a higher concentration of CsCl at the crystal's surface than the bulk, otherwise there would be no concentration gradient resulting in no separation. The freezing of this diffusion boundary layer with a higher CsCl concentration would cause the drip concentration to be higher than the bulk concentration [6]. This diffusion boundary layer concentration would apply to all experimental crystals suggesting that the CsCl concentration of the drips should all be greater than the bulk. This would indicate that the drip removal process is the main reason for variance between crystal drip concentrations relative to the bulk concentrations.

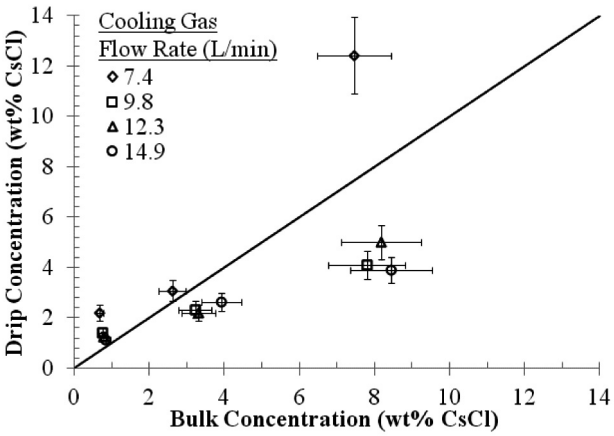

Fig. 11. Drip Concentration vs. Bulk Concentration for Experiments Performed at Initial Concentrations of 1, 3, and 7.5 wt% CsCl in LiCl with 15 min Crystal Growth Times for Varying Cooling Gas Flow Rates.

The effects of initial bulk concentration on crystal growth rate and purified crystal and drip concentration are shown in Fig. 12A and 12B. Fig. 12A shows that the mass of crystal and drip decreases as initial bulk CsCl concentration increases for all cooling gas flow rates with crystal growth times of 15 min. Fig. 12B reveals that as initial bulk CsCl concentration increases, purified crystal and drip concentration increases by less than 0.5 wt% CsCl for the initial bulk concentration range of 1 to 7.5 wt% CsCl with an exception of one data point (Exp. No. 5 with 15 min growth time and 7.4 L/min cooling gas flow rate). This large concentration exists because it has the smallest crystal and drip mass (see Fig. 12A) and would have the most unstable crystal and drip concentration. The instability is because the drip mass fraction would be largest for this data point and the drip's CsCl concentration would be relatively higher than other experiments ran at initial CsCl concentrations lower than 7.5 wt% CsCl. Thus, it is safe to say that initial bulk concentration has a relatively small effect on crystal growth purity within an initial bulk concentration range of 1 to 7.5 wt% CsCl in LiCl.

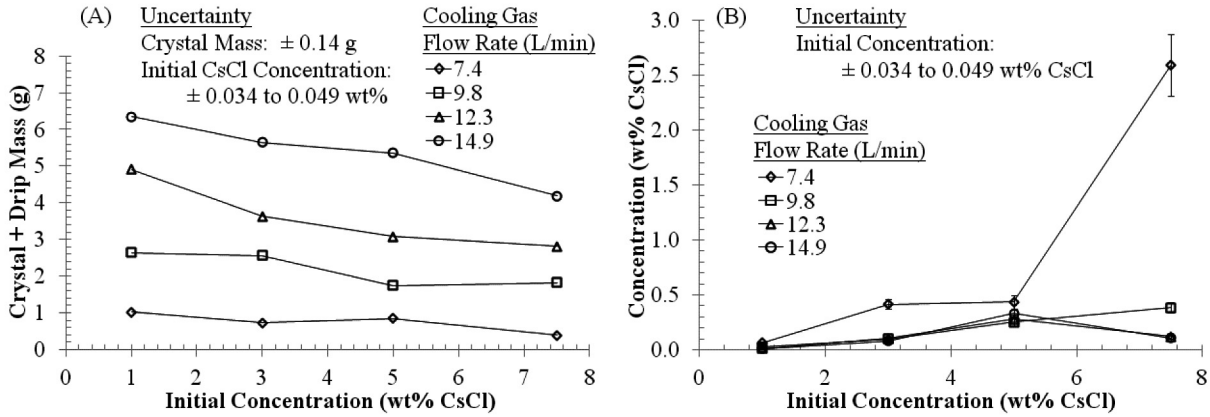

Fig. 12. Purified Crystal and Drip Mass (A) and Concentration (B) vs. Initial Bulk Concentration for Experiments Performed with 15 min Crystal Growth Times for Varying Cooling Gas Flow Rates.

3.2 Crystal Growth Rate Correlations

Since the system is transient with four independent variables—temperature, concentration, position, and time—it is possible to develop correlations describing this system through different dimensionless groups. Three proposed crystal growth rate correlations—(1) mass transfer, (2) heat transfer, and (3) both heat and mass transfer—can be derived based on a natural convective system like cold finger crystal growth. Dimensionless groups to be considered in developing these correlations are shown in Table 2. The

Table 2. Dimensionless Groups Considered for Development of Correlations

Name	Definition	Ratio of Significance
Biot No.	$Bi = \frac{h_{th}\, L}{k_c}$	$\frac{Internal\ thermal\ resistance}{Surface\ thermal\ resistance}$
Fourier No.	$Fo = \frac{k\, t}{\rho\, c_P\, L^2} = \frac{\alpha\, t}{L^2}$	$\frac{Physical\ time}{Thermal\ diffusion\ time}$
Grashof No.	$Gr = \frac{g\, \beta \left\lvert \Delta T \right\rvert L^3\, \rho^2}{\mu^2}$	$\frac{Buoyancy\ force}{Viscous\ force}$
Jakob No.	$Ja = \frac{c_{Pc}\,(T_{Freeze} - T_{Bulk})}{h_{cf}}$	$\frac{Sensible\ energy}{Latent\ energy}$
Lewis No.	$Le = \frac{Sc}{Pr} = \frac{\alpha}{D_{AB}}$	$\frac{Thermal\ diffusion}{Species\ diffusion}$
Nusselt No.	$Nu = \frac{h_{th}\, L}{k}$	$\frac{Convection\ heat\ transfer}{Conduction\ heat\ transfer}$
Prandtl No.	$Pr = \frac{\mu\, c_P}{k}$	$\frac{Viscous\ diffusion}{Thermal\ diffusion}$
Schmidt No.	$Sc = \frac{\mu}{\rho\, D_{AB}}$	$\frac{Viscous\ diffusion}{Species\ diffusion}$
Sherwood No.	$Sh = \frac{h_m\, L}{D_{AB}}$	$\frac{Overall\ mass\ diffusion}{Species\ diffusion}$

where h_{th} = heat transfer coefficient, L = characteristic length = $V^{1/3}$, V = purified crystal volume, k_c = thermal conductivity of purified crystal [8], k = thermal conductivity at T_{Avg} of molten salt [9], T_{Avg} = average temperature in Kelvin = (T_{Freeze} + T_{Bulk}) / 2, T_{Freeze} = freezing temperature of LiCl-CsCl obtained from a phase diagram for given LiCl mole fractions [4], T_{Bulk} = measured molten salt temperature, t = crystal growth time, ρ = density at T_{Avg} of molten salt, c_P = specific heat capacity at T_{Avg} of molten salt and constant pressure, α = thermal diffusivity at T_{Avg} of molten salt at constant pressure, g = gravitational constant (9.81 m/s^2), β = thermal expansion coefficient of the molten salt = $-(\partial\rho/\partial T)_p/\rho$ [7], ΔT = temperature difference between the bulk and solid/liquid interface of the purified crystal = T_{Bulk} - T_{Freeze}, μ = average dynamic viscosity at T_{Avg} of molten salt, c_{Pc} = specific heat capacity of purified crystal, h_{cf} = latent heat of fusion for purified crystal [10], D_{AB} = species diffusion coefficient of CsCl into LiCl, and h_m = mass transfer coefficient.
Note: All material properties are approximated as pure LiCl.

physical equations used to calculate material properties in dimensionless groups are given in Table 3. Experimental values of *Bi*, *Fo*, *Ja*, *Gr*, *Pr*, *Sc*, and *Le* were calculated on average to be on the order of 0.39, 2.8, 0.099, 71,000, 3.5, 390, and 0.009, respectively. These values indicate that (1) lumped capacitance cannot be used to model the system because Bi > 0.1 [7], (2) experimental crystal growth times allow sufficient time for thermal diffusion to take place, (3) sensible energy is less than latent energy indicating a thermodynamic equilibrium upon phase change, (4) buoyant forces are larger than viscous forces, (5) viscous heat diffusion is more dominant than heat conduction, (6) viscous mass diffusion is dominant over species diffusion in this system, and (7) species diffusion dominates thermal diffusion suggesting that the species diffusion boundary layer is thicker than the thermal diffusion boundary layer [7].

In general, *Nu* and *Sh* correlations can be utilized to determine heat and mass convection transfer coefficients (h_{th} and h_m), respectively. Because the variable of interest is the purified crystal mass for this study, a length scale ($L = V^{1/3}$) for these correlations has been manipulated throughout the general form of correlations for natural convective systems; that is, *Nu* or $Sh = a\,(Gr\,Pr\,Sc)^b$. Here, a dimensionless purified crystal mass (η) [7] can be defined as

$$\eta = \frac{m}{m_0} \tag{1}$$

where m is the purified crystal mass and m_0 is the initial LiCl mass in a 30 g LiCl-CsCl molten salt batch. The purified crystal density (ρ_s = 2068 kg/m^3 [3]) can be used to relate crystal mass to the length scale,

$$L = \left(\frac{m}{\rho_s}\right)^{1/3} \tag{2}$$

Then, η can be represented by

$$\eta \propto Nu^3 \text{ and } Sh^3 \tag{3}$$

in terms of mass to provide a typical form of a Nusselt or Sherwood correlation for natural convection; that is,

$$\eta = a\,(Gr\,Pr\,Sc)^b \tag{4}$$

where the third power is being absorbed into the constants a and b. To investigate the independent variable components of Eq. (4), three correlations for heat, mass, and heat & mass transfers have been broken down into the following form:

$$\eta = \alpha\,(Gr^{\beta}\ Pr^{\chi}\ Sc^{\delta}) \tag{5}$$

where α, β, χ, and δ are the constants. The experimental data sets with initial 1, 3, and 7.5 wt% CsCl were selected for curve fitting because of their distribution of purified crystal masses that covered the entire experimental range. After the fitted parameters were calculated from those data sets, the accuracy of these fitted correlations were tested against the experiments with initial 5 wt% CsCl. The root mean square deviation (*RMSD*) was calculated to check the accuracy of each correlation with reference to experimental data values, ranging between 0% and 100%,

$$RMSD = 100 \times \sqrt{\frac{\sum_{i=1}^{n}\left(\frac{\eta_{exp,i} - \eta_{p,i}}{\eta_{exp,i}}\right)^2}{n}} \tag{6}$$

where n is the number of experimental data points and the subscripts *exp*,*i* and *p*,*i* denote experimental and predicted values, respectively. A correlation is most reliable when the *RMSD* is near or equal to zero. In addition, an analysis of the R^2 values for the correlations provides additional insight to the crystal growth behavior. The expression of R is given by:

$$R = \frac{N\sum_i(\eta_{exp,i}\,\eta_{p,i}) - (\sum_i \eta_{exp,i})(\sum_i \eta_{p,i})}{\sqrt{N\sum_i \eta_{exp,i}^2 - (\sum_i \eta_{exp,i})^2}\ \sqrt{N\sum_i \eta_{p,i}^2 - (\sum_i \eta_{p,i})^2}} \tag{7}$$

to indicate the degree of correlation [15]. Hear, a correlation is most reliable when the R^2 value is close to unity. Iterative guess and check procedures were done with the use of *Microsoft Excel* to minimize the *RMSD*. Table 4 provides the resulting values and *RMSD* for all correlations. The convergence of the exponents β and χ suggest that the previous heat transfer correlation is good and that it could take the form of $\eta = a\,Ra^b$ where Ra is the Rayleigh number

Table 3. Equations used to Calculate Molten Salt Properties at T_{Avg}

Variable	Equation	Units	References
Average density	$\rho = 1.88\times10^3 - 0.433T_{Avg}$	kg/m^3	[11]
Average dynamic viscosity	$\mu = (1.09\times10^{-4})\exp[1.91\times104/(8.31T_{Avg})]$	kg/(s·m)	[11]
Average specific heat capacity	$c_P = (7.32\times10^4 - 9.05T_{Avg})/42.4$	J/(kg K)	[12]
Species diffusion coefficient	$D_{AB} = (9.30\times10^{-8})\exp[-6.44\times10^3/(1.99T_{Avg})]$	m^2/s	[13] & [14]

and is the product of *Gr* and *Pr* representing a ratio of buoyancy to viscous forces [16]. A plot of η verses *Gr* provide a visual representation of the fitted correlations to the experimental data performed with initial 1, 3, and 7.5 wt% CsCl (see Fig. 13).

When using these fitted correlations to predict the data obtained from experiments performed with initial 5 wt% CsCl, the *RMSD* values had approximately a 60% increase for the prediction (see Table 5). Fig. 14 shows that the correlation is mainly over predicting the experimental data sets except the two data points for crystal growth times of 15 and 30 min and are most likely due to human error in experiments. It would be expected that Exp. No. 4 with 30 min growth time and 14.9 L/min cooling gas flow rate would be relatively larger than other crystals because of the extended crystal growth time compared to other experiments. The plot also confirms previous observations that cooling gas flow rate has the greatest effect on the crystal growth rate compared to initial CsCl concentration and crystal growth time, indicated by the segregated grouping for each cooling gas flow rate along the three correlation profiles; that is, data becomes more scattered for higher cooling gas flow rates.

Table 4. Three Proposed Dimensionless Purified Crystal Mass Correlations with Respective α, β, χ, δ, R^2, and *RMSD* Values for Experiments Performed with Initial 1, 3, and 7.5 wt% CsCl

Effects	Correlation	α	β & χ	δ	R^2	*RMSD*
Heat Transfer	$\eta = \alpha\,(Gr^{\beta}\,Pr^{\chi})$	1.07×10^{-9}	1.46	0.524	0.908	13.69
Mass Transfer	$\eta = \alpha\,(Gr^{\beta}\,Sc^{\delta})$	2.94×10^{-10}	1.46	0.524	0.908	13.69
Heat & Mass Transfers	$\eta = \alpha\,(Gr^{\beta}\,Pr^{\chi}\,Sc^{\delta})$	4.67×10^{-11}	1.46	0.524	0.905	13.74

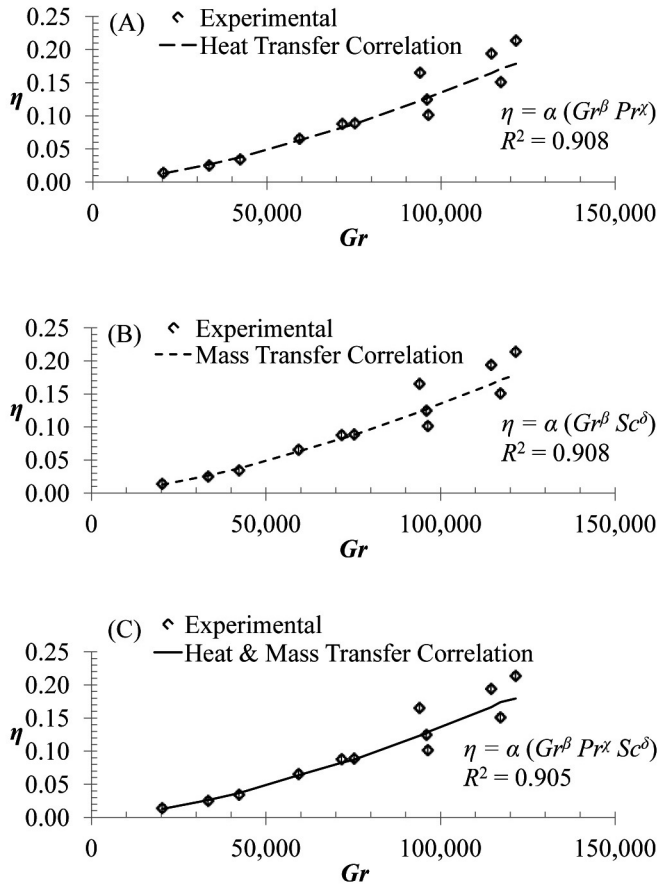

Fig. 13. η vs. *Gr* for: (A) Heat Transfer, (B) Mass Transfer, and (C) Heat and Mass Transfer Correlations Fitted to Experimental Data Performed with Initial 1, 3, and 7.5 wt% CsCl.

3.3 Potential Scale-up and Application

It is possible to envision a potential scale-up scenario for cold finger melt crystallization separation to an existing bench scale oxide reduction setup. An example of this application can be applied to the current process at Idaho National Laboratory. A general planning process has been developed to explore potential purified electrolyte production rates. This bench scale oxide reduction setup was used to process used nuclear fuel. Here, the used nuclear fuel was placed in a 700 g batch of LiCl-Li_2O electrolyte with 1 wt% Li_2O in a MgO crucible that measured 10 cm in diameter and 11 cm in height [1]. The oxide reduction anode and cathode assembly is removable so a cold finger assembly can be used to purify a batch of used electrolyte while the oxide reduction process is off line and removed from the crucible. The maximum number of cold fingers that can fit in the crucible without changing the natural crystal growth shape is seven. The scale-up scenario simulated the concentration of a 700 g batch of used LiCl-CsCl electrolyte from 5 to 7.5 wt% CsCl with 7 cold fingers operating at the aforementioned optimum crystal growth time of 15 min and cooling gas flow rate of 14.9 L/min. The electrolyte was concentrated to 7.5 wt% CsCl so that the effects of initial CsCl concentration could be accounted for by interpolating purified crystal mass and concentration values for each consecutive crystal growth cycle. It would require 7 growth cycles with an approximate total operation time of 105 min to concentrate used electrolyte from 5 to 7.5 wt% CsCl. Given this scale-up scenario, a potential purified electrolyte production rate of 136 g/hr was calculated with an associated purity calculation of 0.24 wt% CsCl.

To determine if cold finger melt crystallization is an economically feasible method for commercial use, additional experimentation and analysis must be performed. Cold finger melt crystallization was developed as a potentially faster melt crystallization separation method for zone freezing, a reverse Bridgman crystal growth separation technique. Used oxide reduction electrolyte contains additional undesirable fission products like Cs such as barium (Ba), strontium (Sr), rubidium (Rb), tellurium (Te), and europium (Eu) which may affect the production rate and purity of processed electrolyte [1]. It is potentially possible that the freezing temperatures of fission products other than Cs in the actual used oxide reduction electrolyte are close to the freezing point of the desired LiCl causing separation purity problems. For example, $BaCl_2$-LiCl has a eutectic melting temperature of 514 ºC at approximately 75 mol% of LiCl. By using this example, if a small amount of CsCl was to be present, then it is expected that a layer of $BaCl_2$ will be formed prior to a CsCl layer. Understanding

Table 5. Three Proposed Dimensionless Purified Crystal Mass Correlations with Respective α, β, χ, δ, R^2, and *RMSD* Values of Predicting Experiments Performed with Initial 5 wt% CsCl

Effects	Correlation	α	β & χ	δ	R^2	*RMSD*
Heat Transfer	$\eta = \alpha (Gr^{\beta} Pr^{\chi})$	1.07×10^{-9}	1.46	0.524	0.844	22.5
Mass Transfer	$\eta = \alpha (Gr^{\beta} Sc^{\delta})$	2.94×10^{-10}	1.46	0.524	0.844	22.5
Heat & Mass Transfers	$\eta = \alpha (Gr^{\beta} Pr^{\chi} Sc^{\delta})$	4.67×10^{-11}	1.46	0.524	0.856	21.4

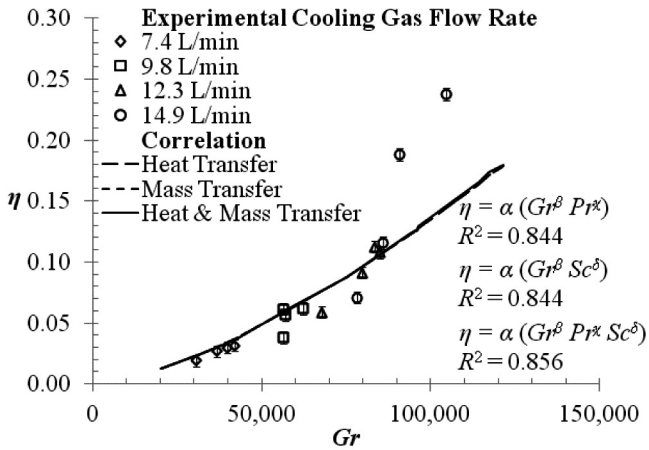

Fig. 14. η vs. *Gr* for Correlations Predicting Experimental Data Performed with Initial 5 wt% CsCl.

this thermodynamic behavior would allow a researcher to possibly control the crystal growth process and the adjustment of operational cost accordingly.

4. SUMMARY

Cold finger melt crystallization separation experiments under different parametric effects were proposed and conducted to further develop pyrochemical technology through experimentation and correlation analysis. Results of experiments with initial 5 wt% CsCl concentration showed that the optimal cooling gas flow rate and crystal growth time of this experimental setup was 14.9 L/min and 15 min, respectively, producing a 0.33 wt% CsCl crystal purity at a production rate of 0.36 g/min. Experimental results for initial concentrations of 1, 3, and 7.5 wt% CsCl at the aforementioned coolant flow rates for separation times of 15 min were analyzed and showed that, in majority, the change in purified crystal concentration was less than 0.5 wt% CsCl as initial CsCl concentration increased from 1 to 7.5 wt% CsCl.

Three crystal growth rate correlations were developed to better understand crystal growth rate behavior and determine the effects of heat and mass transfers on the cold finger melt crystallization separation process. Analysis of the three correlations showed that they predict experimental data well for slower cooling gas flow rates and not as well for faster cooling gas flow rates because operation at slower cooling gas flow rates is closer to thermodynamic equilibrium then operation at faster cooling gas flow rates. The overall analyses of this work has revealed two major discoveries of cold finger melt crystallization as a viable means of purifying used electrolytic oxide reduction electrolyte. The first significant discovery was the effect of a CsCl concentrated drip formation on purified crystal that decreases crystal purity, especially for smaller crystal formations where drip mass fractions are larger. The second significant discovery shown by the analyses was that cooling gas flow rate controls the production rate of cold finger separation more than both initial CsCl concentration and crystal growth time.

To demonstrate possible scale up of this process, electrolytic oxide reduction results reported by Hermann and co-workers [1] were selected and tested to show the number of cold finger to be used, the operating time, and the amount of recycled salt for this process. Giving the proposed setup, the production rate will be about 135 g/hr with 0.24 wt% CsCl impurities in the LiCl crystal. Additional experimentation and analysis would be necessary to help determine the economic feasibility of commercializing cold finger melt crystallization separation as a method of purifying used oxide reduction electrolyte. With an understanding of thermodynamic behaviors, it will be possible to characterize and control crystallized layer formations.

ACKNOWLEDGMENTS

Acknowledgements go out to Debbie Lacroix with the Center for Advanced Energy Studies (CAES) for elemental analysis of all experimental samples and the CAES facility for use of their Radiochemistry Laboratory. This work was funded by the Laboratory Directed Research and Development Program of Idaho National Laboratory, administered by the Center for Advanced Energy Studies, under the Department of Energy Idaho Operations Office Contract DE-AC07-05ID14517.

REFERENCES

[1] S. D. Herrmann, S. X. Li, M. F. Simpson, and S. Phongikaroon, "Electrolytic Reduction of Spent Nuclear Oxide Fuel as Part of an Integral Process to Separate and Recover Actinides from Fission Procucts." *Separation Science and Technology*, **vol. 41**, pp. 1965-1983 (2006).

[2] Y. Cho, G. Park, H. Lee, I. Kim, and D. Han, "Concentration of Cesium and Strontium Elements Involved in a LiCl Waste Salt by a Melt Crystallization Process." *Nuclear Technology*, **vol. 171**, pp. 325-334 (2010).

[3] R. C. Weast, *Handbook of Chemistry and Physics*, p. B-125, CRC Press Inc., Cleveland (1976).

[4] "*FactSage*," http://www.factsage.cn/fact/documentation/FTsalt/CsCl-LiCl.jpg, Accessed 21 January 2013.

[5] B. H. Park, I. W. Lee, and C. S. Seo, "Electrolytic reduction behavior of U3O8 in a molten LiCl-Li2O salt." *Chemical Engineering Science*, **vol. 63**, pp. 3485-3492 (2008).

[6] R. B. Bird, W. E. Stewart, and E. N. Lightfoot, *Transport Phenomena*, pp. 513-542 and 764-804, John Wiley & Sons Inc., New York (2007).

[7] F. P. Incropera, D. P. Dewitt, T. L. Bergman, and A. S. Lavine, *Fundamentals of Heat and Mass Transfer*, 6th ed., pp. 8, 259-263, 374-381, and 559-597, John Wiley & Sons Inc., Hoboken (2007).

[8] V. A. Khokhlov, A. O. Kodintseva, and E. S. Z. Filatov, "Anomalous" Thermal Conductivity of Crystalline Alkali Halides Close to Their Melting Point." *Naturforsch., A: Astrophys., Phys. Chem*., **vol. 48A**, pp. 595-598 (1993).

[9] Y. Nagasaka, N. Nakazawa, and A. Nagashima, "Experimental determination of the thermal diffusivity of molten alkali halides by the forced Rayleigh Scattering method. I. molten LiCl, NaCl, KCl, RbCl, and CsCl." *International Journal of Thermophysics*, **vol. 13**, pp. 555-574 (1992).

[10] D. W. Green and R. H. *Perry, Perry's Chemical Engineers' Handbook*, 8th ed., pp. 2-146 and 2-159, McGraw-Hill, New York (2008).

[11] G. J. Janz, "Thermodynamic and Transport Properties for Molten Salts: Correlation Equations for Critically Evaluated Density, Surface Tension, Electrical Conductance, and Viscosity Data." *Journal of Physical and Chemical Reference Data*, **vol. 17 #2**, pp. 63-289 (1988).

[12] "*National Institute of Standards and Technology (NIST)*," http://webbook.nist.gov/cgi/cbook.cgi?ID=C7447418&Type=JANAFL&Table=on, Accessed 2 July 2013.

[13] G. J. Janz and N. P. Bansal, "Molten Salts Data: Diffusion Coefficients in Single and Multi-Component Salt Systems." *J. Phys. Chem. Ref. Data*, **vol. 11 #3**, pp. 522-523 (1982).

[14] J. M. Prausnitz, R. N. Lichtenthaler, and E. Gomes de Azevedo,

Molecular Thermodynamics of Fluid-Phase Equilibria, 3rd ed., p. 844, Prentice-Hall Inc., Upper Saddle River (1999).
[15] P. R. Bevington, *Data Reduction and Error Analysis for the Physical Sciences*, pp. 122-129, McGraw-Hill Book Company, New York (1969).
[16] Y. A. Cengel and J. M. Cimbala, *Fluid Mechanics Fundamentals and Applications*, 2nd ed., pp. 283-319, McGraw-Hill Companies Inc., New York (2010).